Wind and Temperature Profiles in the Radix Layer: The Bottom Fifth of the Convective Boundary Layer

EDI SANTOSO AND ROLAND STULL

Atmospheric Science Programme, Department of Geography, University of British Columbia, Vancouver, British Columbia, Canada

(Manuscript received 8 January 1997, in final form 13 November 1997)

ABSTRACT

In the middle of the convective atmospheric boundary layer is often a deep layer of vertically uniform wind speed (M_{UL}), wind direction, and potential temperature (θ_{UL}). A radix layer is identified as the whole region below this uniform layer, which includes the classic surface layer as a shallower subdomain. An empirical wind speed (M) equation with an apparently universal shape exponent (A) is shown to cause observations from the 1973 Minnesota field experiment to collapse into a single similarity profile, with a correlation coefficient of roughly 0.99. This relationship is $M/M_{UL} = F(z/z_R)$, where F is the profile function, z is height above ground, and z_R is depth of the radix layer. The profile function is $F = (z/z_R)^A \exp[A(1 - z/z_R)]$ in the radix layer ($z/z_R \leq 1$), and $F = 1$ in the uniform layer ($z_R < z < 0.7z_i$). The radix-layer equations might be of value for calculation of wind power generation, wind loading on buildings and bridges, and air pollutant transport.

The same similarity function F with a different radix-layer depth and shape exponent is shown to describe the potential temperature (θ) profile: $(\theta - \theta_{UL})/(\theta_0 - \theta_{UL}) = 1 - F(z/z_R)$, where θ_0 is the potential temperature of the air near the surface. These profile equations are applicable from 1 m above ground level to the midmixed layer and include the little-studied region above the surface layer but below the uniform layer. It is recommended that similarity profiles be formulated as mean wind or potential temperature versus height, rather than as shears or gradients versus height because shear expressions disguise errors that are revealed when the shear is integrated to get the speed profile.

1. Structure of the convective mixed layer

The goal of this research is to describe the mean wind speed (M) and potential temperature (θ) profiles within the bottom fifth of the convective boundary layer. Figure 1a identifies layers in the convective mixed layer (ML), using wind speed as an example.

Starting from the top, the free atmosphere is where surface friction is not felt, and the actual wind speed is nearly equal to the geostrophic or gradient wind speed G. This layer is above the boundary layer. Next is the entrainment zone, a region of subadiabatic temperature profiles, overshooting thermals, intermittent turbulence, and wind shear (Deardorff et al. 1980).

Further down is a region where wind speed and direction are nearly uniform with height, z. This is the uniform layer (UL), where the wind speed is M_{UL} and the potential temperature is θ_{UL}. The wind is subgeostrophic because thermals communicate surface drag information via nonlocal transport. Traditionally, the term ''mixed layer'' is reserved for the whole turbulent region between the surface and the average ML top, z_i; hence, we distinguish between the ML and the UL to avoid confusion.

Between the surface and the UL is a radix layer (RxL) of depth z_{RM}. Like the roots of a tree, the radix (Latin for ''root'') layer is where smaller plumes merge into large-diameter ML thermals. It contains the classic surface layer as a subdomain (Fig 1a), as will be explained below. Winds in this layer are zero near the ground, and smoothly increase to become tangent to M_{UL} at the RxL top.

Within the bottom of the RxL is the classic surface layer (SL), the nearly constant flux region where Monin–Obukhov similarity theory applies. The SL is the region where predominantly mechanically generated turbulence within the wall shear flow produces a nearly logarithmic wind profile. Again, we distinguish between the RxL and the SL to avoid confusion because we retain the traditional definition that the SL is that region where Monin–Obukhov similarity applies. Although not the subject of this paper, Zilitinkevich (1994) further subdivides the traditional surface layer into (from bottom up) a mechanical turbulence layer, an alternative turbulence layer, and a free convection layer, where the top two layers combine to form his convective and mechanical layer.

Radix-layer definitions also can be made for potential temperature, as sketched in Fig. 1b. The depth of the

Corresponding author address: Dr. Roland Stull, Atmospheric Science Programme, Dept. of Geography, University of British Columbia, 1984 West Mall, Vancouver, BC, V6T 1Z2, Canada.
E-mail: rstull@geog.ubc.ca

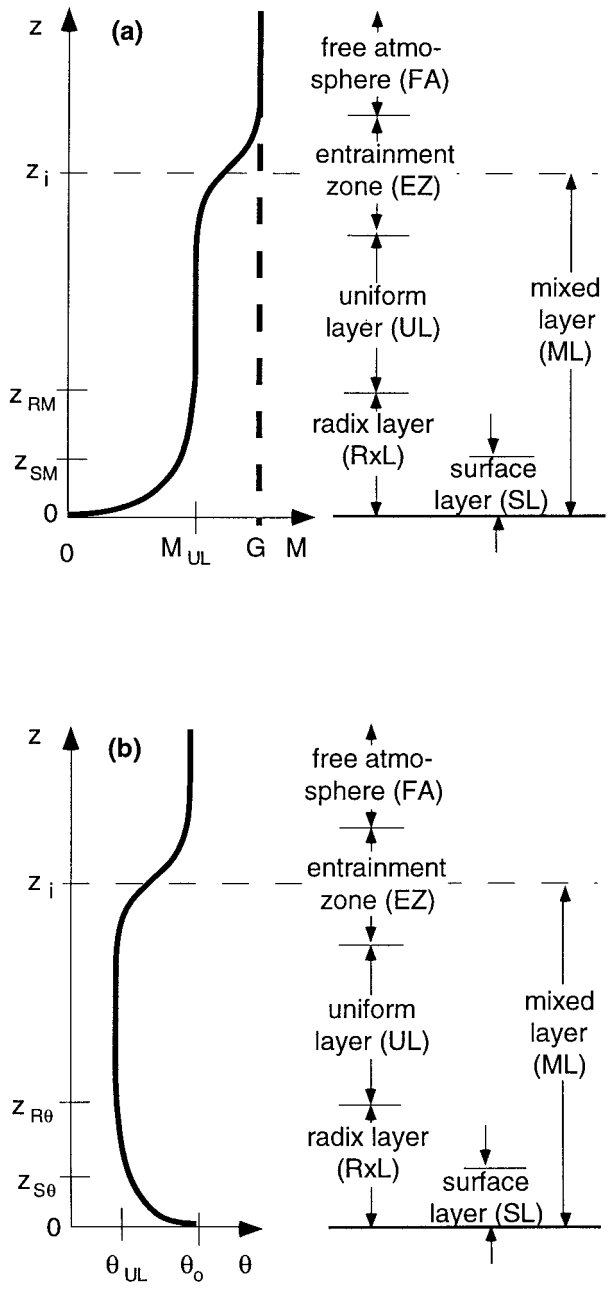

FIG. 1. Idealized profiles showing components of the convective mixed layer for (a) wind M and (b) potential temperature θ. Here, G is geostrophic wind speed.

SL and RxL for temperature can be different than for momentum. For potential temperature, we denote these depths as $z_{S\theta}$ and $z_{R\theta}$, respectively.

Based on these traditional and new definitions, we see that the ML (order of a couple kilometers thick) contains the RxL (hundreds of meters thick) as a subdomain, and the RxL contains the SL (tens of meters thick) as a subdomain. Hence, there is a superposition of layers in the bottom fifth of the convective boundary layer. This is an alternative view to the three-layer model of Garratt et al. (1982), where their surface layer merges directly into the uniform layer.

Because the proposed profile equations will be expressed as a dimensionless similarity theory, section 2 starts by reviewing similarity hypotheses for the bottom of the boundary layer. In section 3 similarity equations for the radix layer are proposed and calibrated against field data. In section 4 there is a first attempt to identify parameters that control the radix-layer depth. The value of similarity wind profiles over similarity shear profiles is discussed in section 5.

2. Similarity hypotheses

a. Surface layer

Most SL similarity theories are based on the following premises:

1) flux is approximately uniform with height (constant flux ± 10%);
2) turbulence consist of ''small eddies,'' causing local transport;
3) turbulence is predominantly generated mechanically by shear flow near the ground, with minor modifications for static stability; and
4) feedback exists between the mean flow and the dominant eddies.

The first premise not only simplifies the theory by allowing flux variations to be neglected but it constrains the depth of applicability to the bottom 10% of the ML, assuming heat flux decreases roughly linearly with height during near-free convection. The second premise suggests that ML depth z_i should not be relevant. The third premise implies that surface roughness length z_0 is important. The fourth premise is discussed later.

Most classic SL similarity equations are strongly dependent on the surface but are virtually independent of factors higher in the ML. Typically lacking is dependence on ML depth, temperature within the UL, winds within the UL, and geostrophic wind speed. For this reason, we cannot expect the SL equations to merge smoothly into the UL because no information about the UL is included in those equations. Panofsky (1978) points out that convective-matching-layer and free-convection-layer formulations (Priestley 1955; Kaimal et al. 1976) fail near the bottom of the UL, where the shear and potential-temperature gradient approach zero.

This situation is illustrated in Fig. 2, where the abscissa has been normalized according to the Businger (1971)–Dyer (1974) similarity theory. In this normalization, all the data will collapse to a single curve regardless of static stability in those regions where SL similarity theory is valid. While Fig. 2a shows that SL similarity works well in the bottom 40 m of the ML for the Minnesota dataset (to be described in more detail later), Fig. 2b shows that SL theory is less successful higher in the RxL and in the UL. Namely, the classic

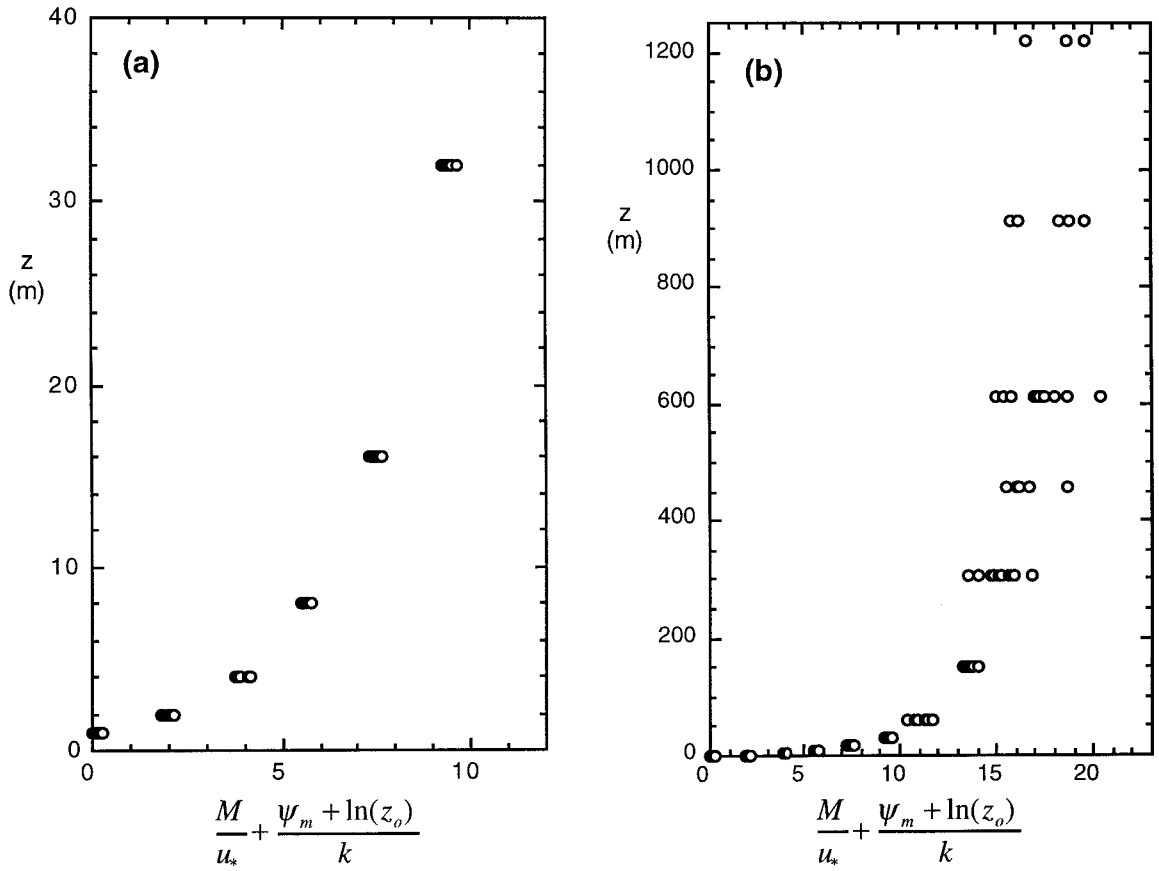

FIG. 2. Wind profiles for all 11 runs of the Minnesota campaign. Abscissa is normalized using surface-layer similarity, where z_0 is aerodynamic roughness length, $k = 0.4$ is von Kármán's constant, and ψ_m is the integrated wind profile stability–correction function of Businger and Dyer: (a) within the surface layer and (b) within the radix and uniform layers.

surface layer does not extend up to the base of the UL for these data, resulting in data points that do not collapse onto a single curve.

Monin–Obukhov similarity theory has been the favored tool for finding wind and temperature profiles in the SL. Within this theory, dimensionless wind shear as a function of dimensionless height z/L is defined as

$$\phi_m\left(\frac{z}{L}\right) \equiv \frac{kz}{u_*}\frac{\partial M}{\partial z}, \tag{1}$$

where L is the Obukhov length (negative for a statically unstable BL), k is von Kármán's constant (approximately 0.4), and u_* is the friction velocity. This expression can be integrated to yield the mean wind profile,

$$M(z) = \int_{z'=z_0}^{z} \frac{u_*}{kz'}\phi_m\left(\frac{z'}{L}\right) dz', \tag{2}$$

where z_0 is the aerodynamic roughness length and z' is a dummy of integration. The function ϕ_m varies away from unity as the static stability varies from neutral; however, the functional form of ϕ_m is not known from first principles.

Many empirical estimates of the functional form of ϕ_m have been suggested for the statically unstable surface layer. These forms can be broadly classified into two groups. One group is the modified logarithmic:

$$\phi_m\left(\frac{z}{L}\right) = \alpha\left(\beta - \gamma\frac{z}{L}\right)^{\delta}, \tag{3}$$

where α, β, γ, and δ are arbitrary empirical constants that usually differ from author to author (e.g., Businger et al. 1971; Dyer 1974; Dyer and Bradley 1982; Högström 1988; Frenzen and Vogel 1992).

The other group is the power law:

$$\phi_m\left(\frac{z}{L}\right) = a\left(-b\frac{z}{L}\right)^{c}, \tag{4}$$

where a, b, and c are arbitrary constants that also differ from author to author (e.g., Swinbank 1968; Zilitinkevich and Chalikov 1968; Foken and Skeib 1983; Kader and Yaglom 1990). Both broad groups are a function of z/L, which implies that both tacitly assume that the dom-

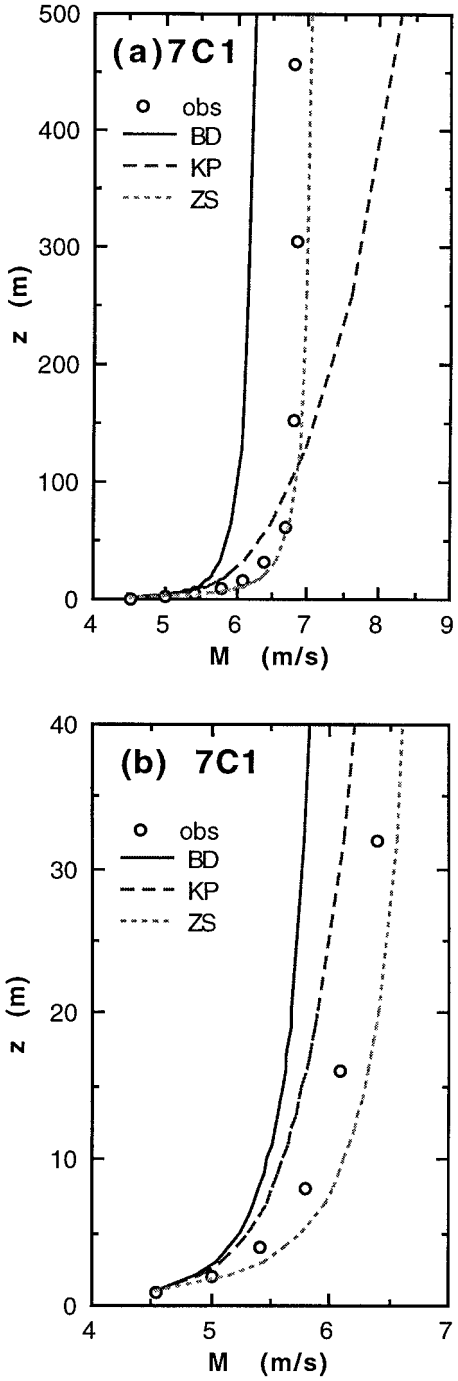

FIG. 3. Wind observations from the Minnesota field experiment run 7C1 compared to three surface-layer models [KP = Kader and Perepelkin 1989; ZS = Sorbjan 1986; BD = Businger–Dyer (Businger et al. 1971)]: (a) above and (b) within the traditional SL. See appendix C for plots of the other runs.

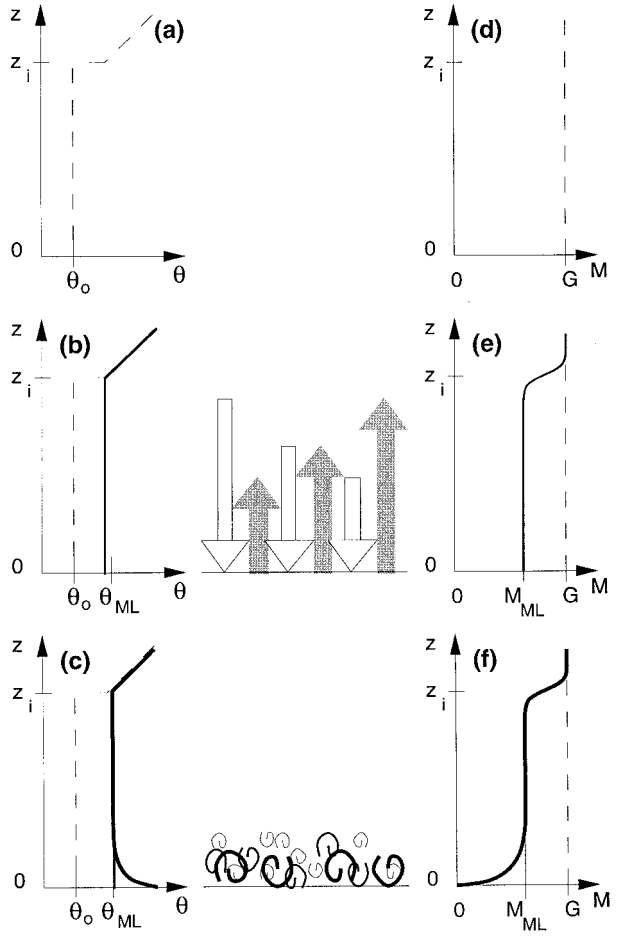

FIG. 4. Potential temperature (left) and wind (right) superposition of transport processes (center) imposed on the background states (a) and (d), by large thermals (b) and (e) in the uniform layer, and smaller shear-driven eddies (c) and (f) in the radix layer (after Stull 1994).

inant generation of turbulence is mechanical, formed by wall shear (Stull 1997).

Some SL similarity equations have been proposed to apply higher into the ML. For example, Fig. 3 compares the SL similarity relationships proposed by Kader and Perepelkin (1989) and Sorbjan (1986, hereafter ZS) to the Minnesota data of run 7C1. Also plotted is an extension of the Businger–Dyer profile equations above the surface layer for comparison. Of the three relationships plotted in Fig. 3, the proposal by Sorbjan appears to work the best above the top of the SL; however, even it has substantial errors as shown in appendix C for all Minnesota runs. The Sorbjan relationship will be discussed in more detail in section 5. The difficulties of most SL theories at heights above the top of the traditional SL provide motivation for the definition of an RxL and suggest that classic profile-matching methods (e.g., Rossby similarity) linking SL profiles with UL profiles are probably not justified.

In closing this brief review of SL similarity, we return to the fourth premise listed at the start of this section. That feedback premise has the following interpretation for flow very near the bottom boundary. Turbulence transports momentum, momentum-flux divergence alters the mean-wind profile, and shear in the mean-wind profile generates small-eddy turbulence. The feedback

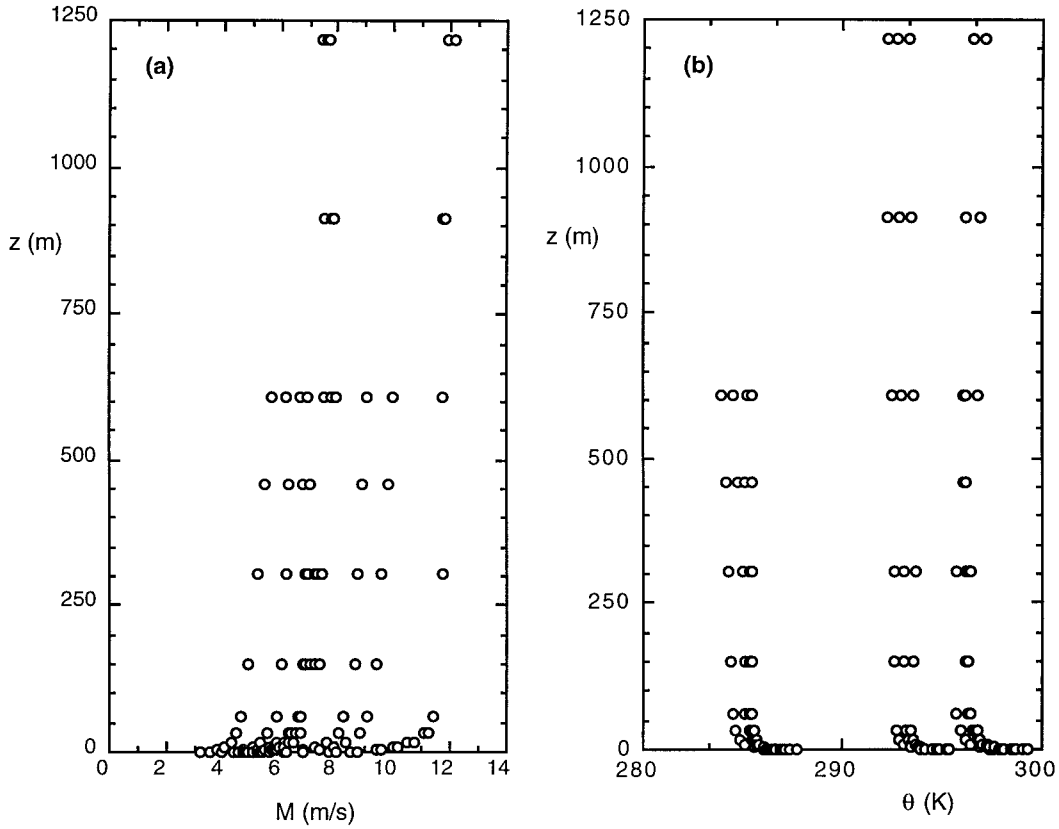

FIG. 5. Raw (a) wind speeds and (b) potential temperatures for all Minnesota runs, showing the range of conditions studied here.

loop is closed, at least for shear-driven surface layers. This is a fundamental, but infrequently discussed, premise underlying SL similarity theory.

b. Radix layer

In the nearly free-convective ML, such feedback is broken. Turbulence still transports momentum, and momentum-flux divergence alters the mean wind profile. However, the mean wind profile does *not* generate large-eddy turbulence. Instead, surface heating generates the large, coherent, thermal structures. Because the thermal structures have a length scale proportional to the ML depth, we can infer that the wind profile in the radix layer must also be a function of z_i.

According to convective transport theory (CTT) for

TABLE 1. Best-fit estimates of parameters in the dimensionless wind, Eq. (7), for $A_1 = 0.0959$, and in the dimensionless potential temperature, Eq. (8), for $A_2 = 0.101$. Also shown for comparison with the radix-layer depths for momentum z_{RM} and temperature $z_{R\theta}$ are the Obukhov length L, and 10% of the mixed-layer depth z_i, which are often used as depth scales for the classic surface layer. Here, UL is the uniform layer, and M_{UL} and θ_{UL} are the wind speed and potential temperature in the UL. The surface potential temperature based on the best-fit profile is θ_0.

	Wind		Potential temperature			Other depth scales	
Run	M_{UL} (m s^{-1})	z_{RM} (m)	θ_{UL} (K)	θ_0 (K)	$z_{R\theta}$ (m)	$-L$ (m)	$0.1z_i$
2A1	11.7	134.5	295.95	304.81	32.22	38.2	125
2A2	11.8	111.8	296.74	305.52	30.27	34.1	162
3A1	9.7	226.7	296.23	304.78	53.07	21.0	231
3A2	8.9	216.5	296.33	302.71	62.17	21.5	230
5A1	(No UL)	(No UL)	285.51	290.39	26.64	8.2	109
6A1	7.4	167.3	292.50	301.16	39.04	5.1	210
6A2	7.6	332.2	293.02	301.43	27.04	5.6	204
6B1	7.7	302.1	293.52	299.39	17.33	19.9	236
7C1	6.8	125.6	284.29	293.16	57.81	7.7	102
7C2	7.0	244.5	284.91	292.38	77.99	11.5	114
7D1	6.2	234.8	285.33	291.16	43.23	11.9	123

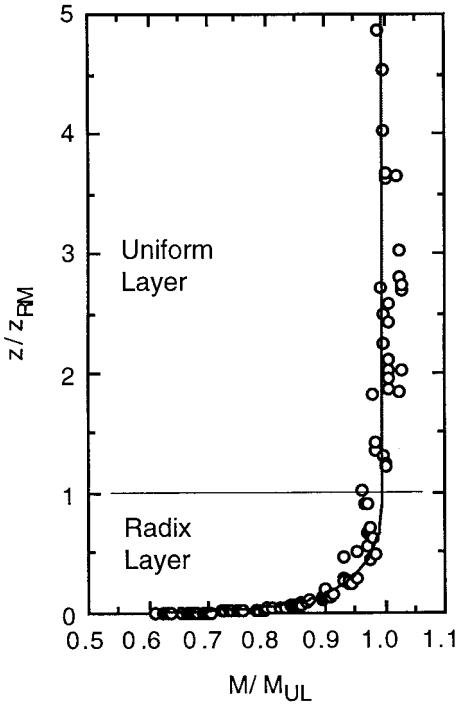

FIG. 6. Data (open circles) from the 10 wind datasets collapse to a common similarity wind profile when radix-layer depth z_{RM} is used to make height z dimensionless, and uniform-layer wind M_{UL} is used to make wind speed M dimensionless. Empirical Eq. (7) is plotted as the solid line, using a "universal" value of $A_1 = 0.0959$. Note that the wind speed Eq. (7) does become zero at the surface, even though there are no data low enough to show it.

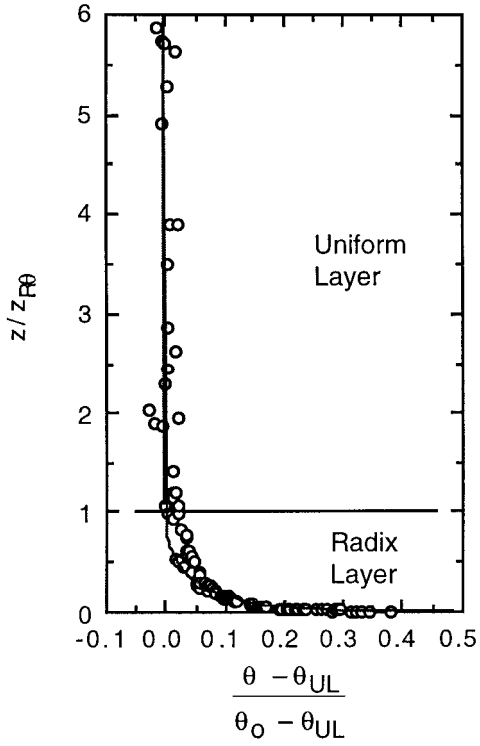

FIG. 7. Data (open circles) from the 11 potential-temperature datasets collapse to a common similarity profile when radix-layer depth $z_{R\theta}$ is used to make height z dimensionless, and temperature difference between the surface skin and the uniform layer ($\theta_0 - \theta_{UL}$) is used to make potential temperature θ dimensionless. Empirical Eq. (8) is plotted as the solid line, using a universal value of $A_2 = 0.101$.

surface fluxes (Stull 1994), the UL is independent of the surface layer. Namely, the UL interacts with the surface directly via the large thermal structures, making it independent of the small-eddy SL and of the roughness length (Fig. 4, after Stull 1994). However, the SL in that previous paper, here better identified as the radix layer, must depend on both roughness length and UL characteristics if it is to become tangent to the UL profile. This also suggests that the RxL is a function of z_i.

CTT identifies a buoyancy velocity scale, $w_B = [(g/T_v)\Delta\theta_{vs}z_i]^{1/2}$, that is valid for free convection. It is proportional to the Deardorff velocity, $w_* = [(g/T_v)\overline{w'\theta'_{vs}}z_i]^{1/3}$, where g is gravitational acceleration, subscript s denotes a surface value, T_v is average virtual temperature, $\Delta\theta_{vs}$ is the virtual potential temperature difference between the surface skin and UL, and $\overline{w'\theta'_{vs}}$ is the surface value of vertical flux of virtual potential temperature, which is similar to a buoyancy flux or a kinematic heat flux. The buoyancy velocity will be utilized later in the paper.

3. Radix-layer wind and temperature profiles

a. Profile equations in the radix layer

For the purpose of the similarity analysis in the RxL/ML system, we hypothesize here that RxL depths (z_{RM} and $z_{R\theta}$) are the relevant height scales and that the winds and temperatures in the UL (M_{UL} and θ_{UL}) are the relevant velocity and temperature scales. After testing several candidate functions, the following empirical profile equations were selected for further study based on their close agreement with the data.

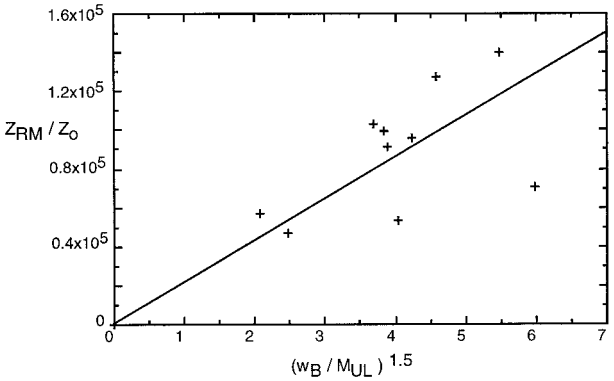

FIG. 8. Linear regression of dimensionless RxL depth z_{RM} for wind against a dimensionless group (w_B/M_{UL}) that is proportional to the square root of the mixed-layer Richardson number (Stull 1994), where z_0 is the aerodynamic roughness length, w_B is the buoyancy velocity, and M_{UL} is the wind speed in the uniform layer.

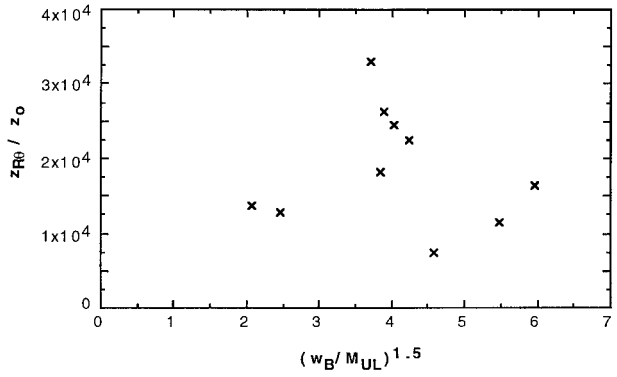

FIG. 9. Dimensionless potential temperature RxL depth $z_{R\theta}$ shows little correlation when plotted against the RxL dimensionless group that was successful for wind.

Equations for wind and potential temperature in the RxL are

$$M = \begin{cases} M_{\mathrm{UL}}\left(\dfrac{z}{z_{\mathrm{RM}}}\right)^{A_1} \exp\left[A_1\left(1-\dfrac{z}{z_{\mathrm{RM}}}\right)\right], & z \le z_{\mathrm{RM}}, \\ M_{\mathrm{UL}}, & z > z_{\mathrm{RM}} \end{cases} \tag{5}$$

and

$$\theta - \theta_{\mathrm{UL}} = \begin{cases} (\theta_0 - \theta_{\mathrm{UL}})\left\{1-\left(\dfrac{z}{z_{R\theta}}\right)^{A_2} \exp\left[A_2\left(1-\dfrac{z}{z_{R\theta}}\right)\right]\right\}, \\ \qquad z \le z_{R\theta}, \\ 0, \qquad z > z_{R\theta}, \end{cases} \tag{6}$$

where A_1 and A_2 are empirical constants and θ_0 is the potential temperature of the air near the surface.

Note that both sets of equations above satisfy the desired constraint that the partial derivative of the parameters (M or θ) with respect to z is zero at the top of the radix layer, z_R. Both sets of the equations also show that the mean profiles and the vertical gradients are continuous and smoothly merge at the top of the RxL. Namely, the RxL profiles are tangent to the UL at a finite height, as observed, rather than asymptotically approaching the UL at infinite height, or rather than crossing the UL at an arbitrary matching height (Panofsky 1978).

b. Calibration against Minnesota data

To locate the top of the RxL, vertically contiguous mean (time averaged) wind speed and temperature data are needed from near the surface through the interior of the ML. Many field experiment datasets do not satisfy this requirement because of the artificial discontinuity created when time-averaged surface-layer data from masts or towers are combined with instantaneous rawinsonde observations above (Clarke and Brooke 1979). Also, many wind profiler systems do not give robust wind-speed measurements below 100–200 m.

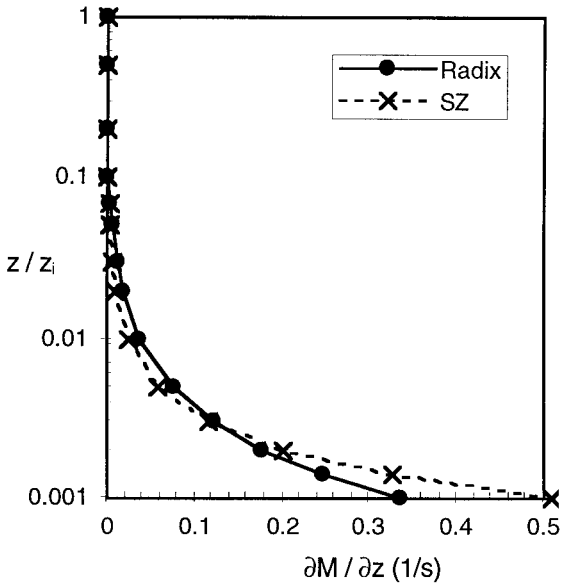

FIG. 10. Comparison of wind shear profiles from Sorbjan (ZS) and from Eq. (10, radix) for typical conditions at Minnesota (z_i = 2000 m, z_{RM} = 200 m, L = −20 m, M_{UL} = 10 m s^{-1}, and w_* = 2 m s^{-1}). The differences are subtle but significant when integrated over height to get wind speed.

However, published data from the 1973 Minnesota field experiment (Izumi and Caughey 1976) are satisfactory. The instrument platforms included a combination of a 32-m tower and sensors at fixed locations on the cable of a tethered balloon. Similar averaging times of 75 min were used at all heights from near the surface through the midmixed layer, yielding profiles of wind and temperature that are self-consistent, smooth, and contiguous. There were 11 datasets (''runs'') that were obtained during the Minnesota experiment. The site was a flat, recently harvested, and plowed farm square-mile section (1.609 km on a side) with no vegetation close by, a roughness length of $z_0 \approx 2.4$ mm, elevation of 255 m above sea level, at location 48°34′N, 96°51′W. A uniform fetch of 10 km existed to the north, which was the predominant wind direction. A more detailed description of the site, instruments, and experimental procedures can be found in Izumi and Caughey (1976) and Kaimal et al. (1976). Appendix A (Table A1) lists key dates, times, and scales for the 11 runs. Figure 5 shows the range of wind speeds and potential temperature profiles present during the runs.

A nonlinear regression (Bevington 1969; Press et al. 1992) is used to determine best-fit parameters M_{UL}, z_{RM}, and A_1 for wind; and θ_0, θ_{UL}, $z_{R\theta}$, and A_2 for potential temperature, for each dataset from the Minnesota experiment. An iterative process is used to minimize the sum of squared deviations between the regression equation (RxL and UL taken together) and the data. Best-

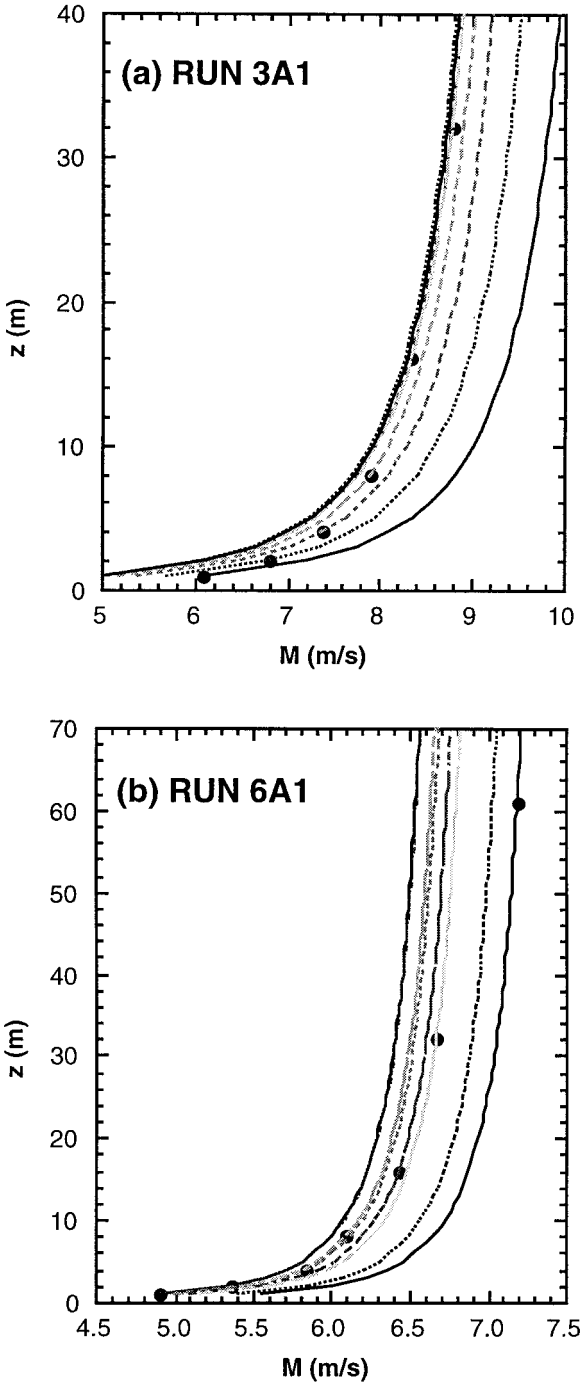

FIG. 11. Wind speed M profiles observed (data points) and found by integrating the Sorbjan (1986) profile relationship (curves) up and down from each data point.

fit estimates of the parameters are listed in appendix B for each of the 11 datasets.

c. Universal constants

Using all the Minnesota runs, parameter $A_1 = 0.095 \pm 0.011$ (mean plus or minus standard deviation) for wind speed, and $A_2 = 0.104 \pm 0.009$ for potential temperature (see appendix B). One wind dataset (run 5A1) did not have a UL in wind speed and, hence, was excluded from the wind speed analysis of this study because no top to the RxL could be found. The relatively small variations in A over the wide range of wind speeds (Fig. 5a), potential temperatures (Fig. 5b), and ML depths suggest that they might be universal. We will make the assumption of universality. Instead of averaging the previously calculated A values to find the universal value, we rearrange the profile equations into a dimensionless form and apply the nonlinear regression to the full set of 10 or 11 runs grouped together as one run. This allows us to find the best-fit A values for a superset of data consisting of the whole Minnesota experiment. This is a more stringent test because it demands similarity simultaneously over a wide variety of wind and depth regimes. That is, while any single dataset might cluster tightly around the curve, the superset is more likely to have scatter (i.e., unexplained variance) if the theory was poor.

First, reframe the wind and temperature profile equations in nondimensional form:

$$\frac{M}{M_{\rm UL}} = \begin{cases} \left(\dfrac{z}{z_{\rm RM}}\right)^{A_1} \exp\left[A_1\left(1 - \dfrac{z}{z_{\rm RM}}\right)\right], \\ \qquad z \le z_{\rm RM}, \\ 1, \qquad z > z_{\rm RM}, \end{cases} \tag{7}$$

and

$$\frac{\theta - \theta_{\rm UL}}{\theta_0 - \theta_{\rm UL}} = \begin{cases} 1 - \left(\dfrac{z}{z_{R\theta}}\right)^{A_2} \exp\left[A_2\left(1 - \dfrac{z}{z_{R\theta}}\right)\right], \\ \qquad z \le z_{R\theta}, \\ 0, \qquad z > z_{R\theta}. \end{cases} \tag{8}$$

The ''universal'' A values are computed using nonlinear least squares analysis, as before, between $M/M_{\rm UL}$ versus $z/z_{\rm RM}$ for the 10 valid wind runs taken together as one large dataset. Similarly, nonlinear regression is used for $(\theta - \theta_{\rm UL})/(\theta_0 - \theta_{\rm UL})$ versus $z/z_{R\theta}$ using data from all 11 temperature runs taken together as one large dataset. The A values are determined such that $M/M_{\rm UL}$ approaches one as $z/z_{\rm RM}$ approaches one, and $(\theta - \theta_{\rm UL})/(\theta_0 - \theta_{\rm UL})$ approaches zero as $z/z_{R\theta}$ approaches one.

The resulting best-fit values are $A_1 = 0.0959 \pm 0.011$ (mean plus or minus standard deviation) for wind and $A_2 = 0.101 \pm 0.009$ for temperature. The correlation coefficient between observed and computed nondimensional equations is $r = 0.992$ for wind speed and $r = 0.986$ for potential temperature. Given these fixed values for A_1 and A_2, the other parameters in the wind and temperature equations found using nonlinear regression are listed in Table 1 for each of the Minnesota runs. Plots of dimensionless wind and temperature profiles

using these universal A values are shown in Figs. 6 and 7.

The parameters listed in Table 1 are not expected to be universal, but they can be functions of external forcings such as geostrophic wind speed G, boundary effects such as z_i and z_0, and scaling variables such as w_B. Most similarity theories incorporate such locally varying nonuniversal parameters, such as the way the Obukhov length is incorporated in SL similarity theory. Note from Table 1 that wind speeds varied by roughly a factor of 2, and RxL depths by a factor of 3, yet the data from each of the 10 wind datasets collapsed into a single similarity curve in Fig. 6. Analogous similarity behavior is evident in Fig. 7 for the 11 temperature datasets. For both wind and temperature, the RxL depth exhibits very little correlation with either classic measures of surface-layer thickness, namely, the Obukhov length L, or 10% of the mixed-layer depth z_i (see Table 1). This latter result differs from the findings of Brutsaert and Sugita (1992) for a different dataset, although their results are for the surface-layer depth rather than the RxL depth.

There are noticeable differences between RxL depths between Table 1 and the tables in appendix B. Because of the gradual approach of the RxL profile to the UL profile, the RxL height is somewhat sensitive to the A parameters and to scatter in the data. Because of this sensitivity, we looked for a better depth scale, such as an integral scale or a half-width height. To date, a better depth scale has not been found. However, the shape of the profile is relatively insensitive to the RxL depth, which means the former sensitivity is not very important.

4. Similarity scaling

What controls RxL depth? From Table 1 it is obvious that RxL depth varies from run to run. It probably also varies from location to location, although the Minnesota case study alone is insufficient to address dependency on roughness length.

In this section we attempt to parameterize RxL depth as a function of constraints and external forcings for the Minnesota case study. These factors include both SL variables such as z_0 and surface buoyancy flux, but they also include ML variables such as z_i. A new field program called Boundary Layer Experiment 1996 (BLX96) was recently conducted to study roughness dependency of RxL characteristics (Stull et al. 1997). Results from this new study will be reported later in a separate paper.

After regressing RxL depth against a wide range of candidate SL and ML variables, we found the following empirical expression to provide the best fit for the Minnesota data:

$$\frac{z_{\mathrm{RM}}}{z_0} = c\left(\frac{w_B}{M_{\mathrm{UL}}}\right)^{3/2}, \tag{9}$$

where the buoyancy velocity w_B was as defined earlier and c is an empirical constant. An expression equivalent to (9) is possible using the Deardorff velocity w_* instead of the buoyancy velocity w_B because the two are linearly related by $w_* \approx 0.08 w_B$ (Stull 1994). The ratio w_B/M_{UL} is the square root of the ''mixed-layer Richardson number'' (Stull 1994). The roughness-length dependence in (9) is tentative, based on theoretical expectations.

Figure 8 shows this regression. The dimensionless slope is $c = 21.4 \times 10^3$ and the correlation is $r = 0.545$, which means that only about 30% of the variance in the data is explained by the regression line. It is clear that additional work needs to be done to identify the factors that control the RxL depth.

The RxL depth for temperature, $z_{R\theta}$, shows even more scatter when plotted (Fig. 9) against the same parameters as for z_{RM}. Also, there was very little correlation ($r = 0.145$) between z_{RM} and $z_{R\theta}$. This might be expected because the wind speed is very highly constrained between zero at the surface and the geostrophic wind aloft, but the temperature profile floats as both the surface skin temperature and the UL temperature increase during the day.

5. Wind profiles versus shear profiles

During this work, it became apparent that inaccuracies of wind profile relationships are hidden when those profiles are expressed in terms of wind shear. However, when those profiles are integrated with height to get the actual wind speeds, the errors are revealed and can accumulate to cause substantial discrepancies between the observed wind speed and the parameterized profile. This is unfortunate because for many practical purposes, such as wind loads on structures, pollutant transport, and wind power generation, it is the speed and not the shear that is needed.

As an example, Fig. 10 compares the wind shear using the Sorbjan (ZS 1986) relationship [his Eq. (38)], and using the radix ralationship, which is

$$\frac{\partial M}{\partial z}\frac{z_{\mathrm{RM}}}{M_{\mathrm{UL}}} = A_1\left(1-\frac{z}{z_{\mathrm{RM}}}\right)\left(\frac{z}{z_{\mathrm{RM}}}\right)^{A-1}\exp\left[A_1\left(1-\frac{z}{z_{\mathrm{RM}}}\right)\right], \quad z \le z_{\mathrm{RM}}$$
$$= 0, \qquad z > z_{\mathrm{RM}}. \tag{10}$$

The difference between these two curves is subtle; it is not easy to discriminate between the two relationships. However, when integrated over height to get wind speed, the deficiencies of the ZS relationship compared with the RxL formulation become apparent and significant (Fig. 3 and Fig. C1). The radix-layer wind speeds are more accurate over a wider range of heights than the ZS speeds.

One might argue that this is an unfair test because integrating up from a small wind near the surface, such as from zero wind at the roughness height, might amplify small initial errors. To examine this argument, one

can recompute the height integration, but starting at different heights. This process is repeated for each data point in the observed wind profile, generating a set of curves such that each curve exactly passes through one point. If the profile similarity theory is valid, then all of the curves should lie nearly on top of each other.

Examples of the integrated ZS wind-speed profiles are shown in Fig. 11, for runs 3A1 and 6A1. Most of the curves do not lie on top of each other. Furthermore, the direction of the error is not consistent: run 3A1 has less shear than the integrated ZS curves, while run 6A1 has more shear. We repeated this exercise for each of the Minnesota runs and found magnitudes of ZS wind-speed errors of roughly ± 3.0 m s^{-1} for runs 2A1, 2A2; ± 1.0 m s^{-1} for runs 3A1 and 3A2; ± 0.7 m s^{-1} for runs 6A1, 6A2, 6B1, and 7C2; and ± 0.3 m s^{-1} for runs 7C1 and 7D1. This compares to wind-speed errors of ± 0.3 m s^{-1} or less for all runs using RxL Eq. (5), as already plotted in Fig. 6.

Thus, it appears that wind speed gives a more sensitive test of the accuracy of a similarity relationship than does shear. We recommend that future proposals for similarity relationships be tested in their integrated form, such as wind speed profiles.

6. Summary and recommendations

Equations (7) and (8) describe similarity relationships for wind speed and potential temperature within the whole radix layer. The radix layer is identified as the region between the surface and the base of the uniform portion of the convective boundary layer. The top of the radix layer (i.e., the base of the uniform layer) is usually well above the top of the classic surface layer.

Using data from the 1973 Minnesota experiment, the resulting best-fit value for the exponents in Eqs. (7) and (8) are $A_1 = 0.0959 \pm 0.011$ for wind and $A_2 = 0.101 \pm 0.009$ for temperature. These exponents are relatively constant for a wide variety of wind speeds and surface heating, suggesting that they might be universal. The correlation coefficient between observed and parameterized profiles is $r = 0.992$ for wind speed and $r = 0.986$ for potential temperature. This suggestion of universality of equations and exponents should be considered tentative until independent verification tests are published and wind-speed ranges of validity are identified.

The radix-layer depth differs from run to run, analogous to run-to-run variations of surface-layer scales such as the Obukhov length. The radix-layer depth for wind is greater than that for temperature, and there is little correlation between the two. An attempt was made to parameterize the radix-layer depth for wind as a function of the mixed-layer Richardson number; however, the fit was poor, suggesting that more work is needed.

The profile equations proposed here are applicable in the range of $1 \text{ m} < z < 0.7\, z_i$. Thus, they span the previously little-studied region above the top of the surface layer and below the base of the uniform layer, where classic Monin–Obukhov similarity theory performs poorly. Potential applications of better wind speed profiles include wind turbine electrical generation, wind loads on buildings and bridges, and air pollutant transport.

We recommend that profile similarity relationships be presented and tested as wind-speed profiles, rather than as shear profiles. The latter tend to hide or disguise errors and give a false picture of the accuracy of the relationship.

Datasets for independent validation are scarce because of the requirements for time- or space-averaged, not instantaneous, observations from the surface into the midmixed layer. To test the above equations, a new field program (Boundary Layer Experiment 1996) was conducted in July and August 1996 in the central United States (Stull et al. 1997). Special vertical zigzag flight patterns in the University of Wyoming King Air aircraft were flown to measure the mean profiles of wind speed and potential temperature. Results from this new validation will be forthcoming.

Acknowledgments. This work was initiated while both authors were at the University of Wisconsin. The following funding agencies are gratefully acknowledged for their support: U.S. National Science Foundation (NSF ATM-9411467), the U.S. Department of Energy (ARM Grant DE-FG02-9ZER61361), the Canadian Atmospheric Environment Service (AES subventions), and the Canadian Natural Sciences and Engineering Research Council (NSERC operating grants).

APPENDIX A

Scaling Variables for Individual Minnesota Runs

TABLE A1. Dates, times, and boundary layer scaling variables for the Minnesota field experiment. Friction velocity is u_*, Deardorff velocity is w_*, buoyancy velocity is w_B, mixed-layer depth is z_i, Obukhov length is L, surface kinematic heat flux is Q_0, surface-layer temperature scale is $T_* = -Q_0/u_*$, and mixed-layer temperature scale is $\theta_* = Q_0/w_*$. Central Daylight Time (CDT) = UTC − 5 h. The buoyancy velocity w_B was calculated from its definition (see section 2b) using $\Delta\theta_{vs}$ equal to $\theta_{vUL} - \theta_{v0}$ and was not calculated from w_*. Also L was calculated using a von Kármán constant of 0.4.

Run	Time (CDT)	Date (1973)	u_* (m s^{-1})	w_* (m s^{-1})	w_B (m s^{-1})	z_i (m)	$-L$ (m)	Q_0 (K m s^{-1})	T_* (°C)	θ_* (°C)
2A1	1217–1332	10 Sep	0.46	2.00	19.0	1250	38.23	0.196	−0.42	0.10
2A2	1332–1447	10 Sep	0.45	2.23	21.5	1615	34.10	0.209	−0.46	0.09
3A1	1510–1625	11 Sep	0.37	2.41	25.4	2310	20.96	0.186	−0.50	0.08
3A2	1625–1740	11 Sep	0.32	2.06	21.9	2300	21.54	0.116	−0.36	0.06
5A1*	1622–1737	15 Sep	0.19	1.35	*	1085	8.16	0.069	−0.38	0.05
6A1	1401–1516	17 Sep	0.24	2.43	24.3	2095	5.08	0.210	−0.88	0.09
6A2	1516–1631	17 Sep	0.23	2.21	23.6	2035	5.64	0.162	−0.71	0.07
6B1	1652–1807	17 Sep	0.26	1.77	21.3	2360	19.87	0.072	−0.27	0.04
7C1	1415–1530	19 Sep	0.28	1.95	17.2	1020	7.74	0.221	−0.79	0.11
7C2	1530–1645	19 Sep	0.30	1.89	16.7	1140	11.49	0.181	−0.60	0.10
7D1	1650–1805	19 Sep	0.25	1.58	15.2	1225	11.92	0.099	−0.40	0.06

* No uniform layer on this day.

APPENDIX B

Nonlinear Regression Parameters for Individual Minnesota Runs

TABLE B1. Best-fit estimates of the parameters in Eq. (5) for wind speed in the combined radix and uniform layers. Here, M_{UL} is wind speed in the uniform layer, z_{RM} is the radix-layer depth for wind, and A_1 is the exponent parameter.

Run	M_{UL} (m s^{-1})	z_{RM} (m)	A_1
2A1	11.80	115.81	0.107
2A2	11.75	86.02	0.107
3A1	9.72	226.73	0.096
3A2	8.86	219.17	0.095
5A1	5.43	610.00	0.096
6A1	7.42	248.67	0.084
6A2	7.72	894.13	0.075
6B1	7.80	593.42	0.082
7C1	6.79	102.07	0.105
7C2	6.97	212.08	0.101
7D1	6.21	236.90	0.096

TABLE B2. Best-fit estimates of the parameters in Eq. (6) for potential temperature in the combined radix and uniform layers. Here, θ_{UL} and θ_0 are the potential temperatures in the uniform layer and in the air adjacent to the surface, respectively; $z_{R\theta}$ is the radix–layer depth for potential temperature; and A_2 is the exponent parameter for potential temperature.

Run	θ_{UL} (K)	θ_0 (K)	$z_{R\theta}$ (m)	A_2
2A1	296.05	304.92	21.02	0.118
2A2	296.75	305.52	23.78	0.115
3A1	296.23	304.78	54.13	0.100
3A2	296.32	302.71	70.42	0.097
5A1	285.50	290.39	30.76	0.094
6A1	292.52	301.16	29.52	0.115
6A2	293.02	301.43	24.57	0.106
6B1	293.52	299.39	19.06	0.096
7C1	284.29	293.16	59.38	0.100
7C2	284.93	292.38	65.16	0.107
7D1	285.32	291.12	53.14	0.093

APPENDIX C

Comparison of Several Wind-Speed Profile Relationships Against Each Individual Minnesota Run

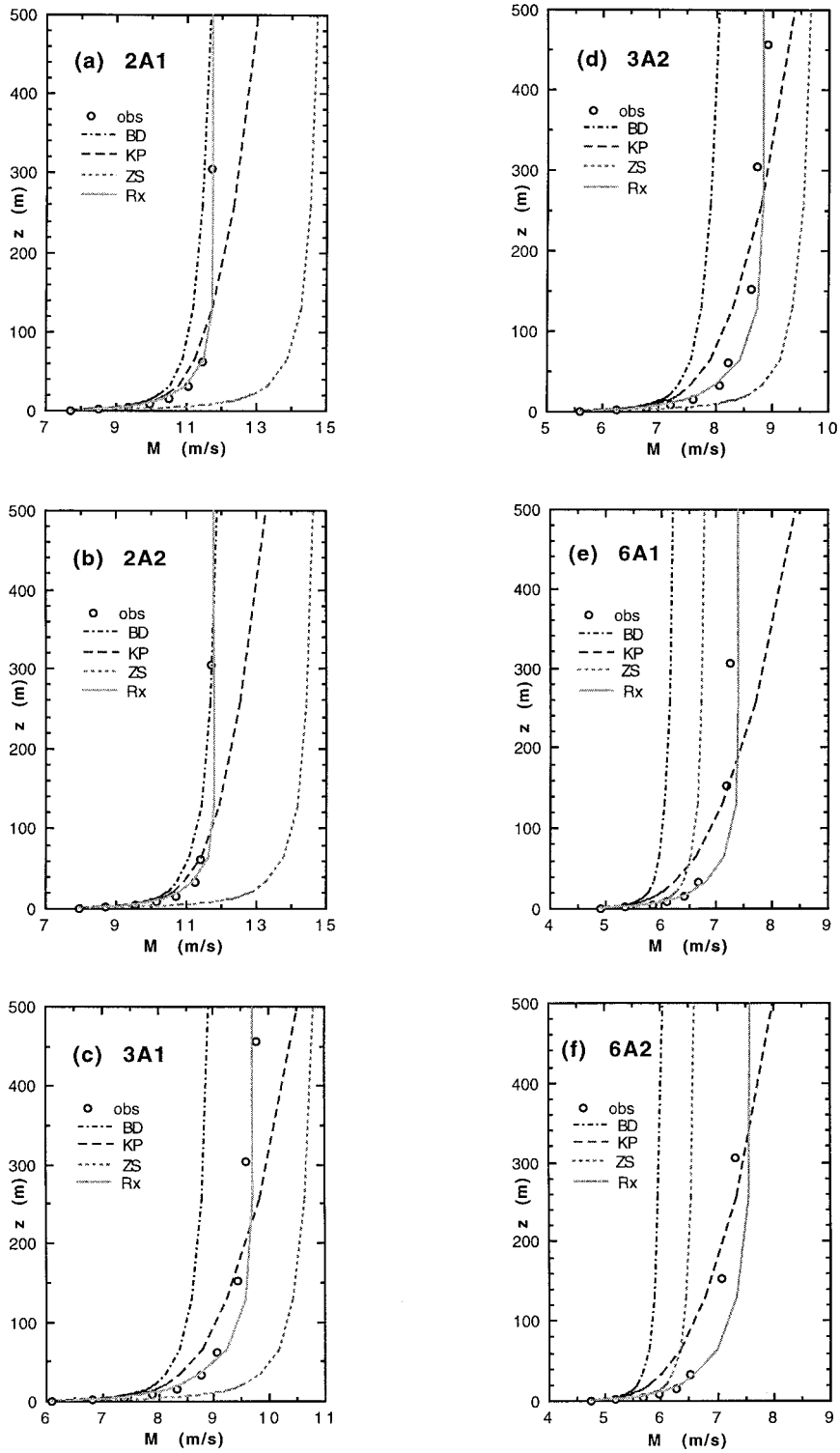

FIG. C1. Wind observations from each of the Minnesota field experiment runs, compared to three surface-layer models [KP = Kader and Perepelkin 1989; ZS = Sorbjan 1986; BD = Businger–Dyer (Businger et al. 1971)] and the RxL model.

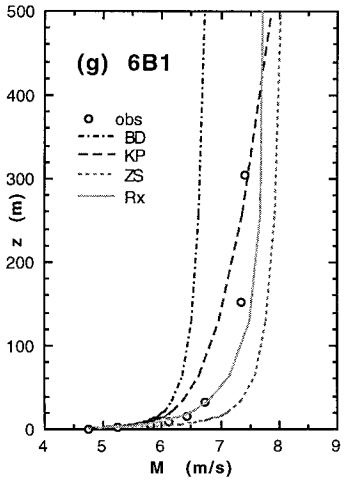

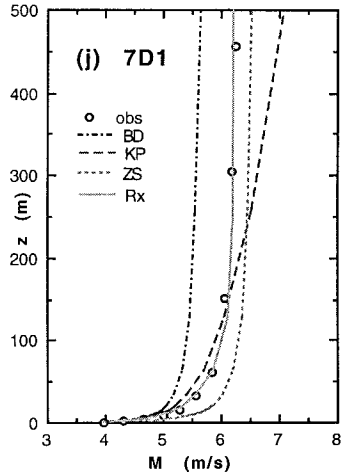

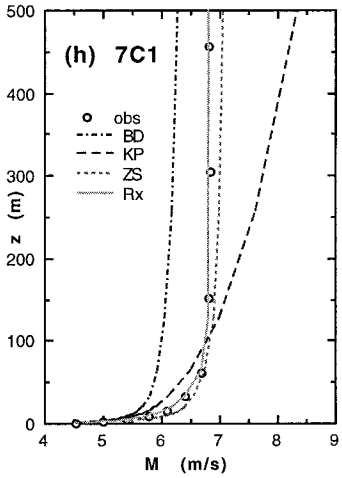

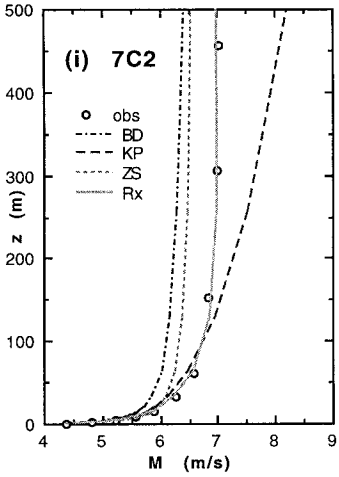

FIG. C1. (*Continued*)

REFERENCES

Bevington, E. H., 1969: *Data Reduction and Error Analysis for the Physical Sciences.* McGraw-Hill, 336 pp.

Brutsaert, W., and M. Sugita, 1992: The extent of the unstable Monin–Obukhov layer for temperature and humidity above complex hilly grassland. *Bound.-Layer Meteor.,* **51,** 383–400.

Businger, J. A., J. C. Wyngaard, Y. Izumi, and E. F. Bradley, 1971: Flux-profile relationships in the atmospheric surface layer. *J. Atmos. Sci.,* **28,** 181–189.

Clark, R. H., and R. R. Brook, 1979: *The Koorin Expedition, Atmospheric Boundary Layer Data over Tropical Savannah Land.* Bureau of Meteorology, Australian Government Publishing Service, 359 pp.

Deardorff, J. W., G. E. Willis, and B. H. Stockton, 1980: Laboratory studies of the entrainment zone of a convectively mixed layer, part 1. *J. Fluid Mech.,* **100,** 41–64.

Dyer, J. A., 1974: A review of flux-profile relationship. *Bound.-Layer Meteor.,* **7,** 363–372.

——, and E. F. Bradley, 1982: An alternative analysis of flux-gradient relationships at the 1976 ITCE. *Bound.-Layer Meteor.,* **22,** 3–19.

Foken, T., and G. Skeib, 1983: Profile measurements in the atmospheric near-surface layer and the use of suitable universal functions for the determination of the turbulent energy exchange. *Bound.-Layer Meteor.,* **25,** 55–62.

Frenzen, P., and C. A. Vogel, 1992: The turbulent kinetic energy budget in the atmospheric surface layer: A review and experimental reexamination in the field. *Bound.-Layer Meteor.,* **60,** 49–76.

Garratt, J. R., J. C. Wyngaard, and R. J. Francey, 1982: Winds in the atmospheric boundary layer—Prediction and observation. *J. Atmos. Sci.,* **39,** 1307–1316.

Högström, U., 1988: Non-dimensional wind and temperature profiles in the atmospheric surface layer: A re-evaluation. *Bound.-Layer Meteor.,* **42,** 55–78.

Izumi, Y., and J. S. Caughey, 1976: Minnesota 1973 atmospheric boundary layer experiment data report. AFCRL-TR-76-0038, 28 pp. [Available from Atmospheric Science Programme, Dept. of Geography, University of British Columbia, 1984 West Mall, Vancouver, BC V6T 1Z2, Canada.]

Kader, B. A., and V. G. Perepelkin, 1989: Effect of unstable stratification on the wind speed and temperature profiles in the surface layer. *Atmos. Oceanic Phys.,* **25,** 583–588.

——, and A. M. Yaglom, 1990: Mean fields and fluctuation moments in unstably stratified turbulent boundary layer. *J. Fluid Mech.,* **212,** 637–667.

Kaimal, J. C., J. C. Wyngaard, D. A. Haugen, O. R. Cote, and Y. Izumi, 1976: Turbulence structure in the convective boundary layer. *J. Atmos. Sci.,* **33,** 2152–2169.

Panofsky, H. A., 1978: Matching in the convective planetary boundary layer. *J. Atmos. Sci.,* **35,** 272–276.

Press, W. H., B. P. Flannery, S. A. Teukolsky, and W. T. Vetterling, 1992: *Numerical Recipes in FORTRAN: The Art of Scientific Computing.* 2d ed., Cambridge University Press, 963 pp.

Priestley, C. H. B., 1955: Free and forced convection in the atmosphere near the ground. *Quart. J. Roy. Meteor. Soc.,* **81,** 139–143.

Sorbjan, Z., 1986: On similarity in the atmospheric boundary layer. *Bound.-Layer Meteor.,* **34,** 377–397.

Stull, R. B., 1994: A convective transport theory for surface fluxes. *J. Atmos. Sci.,* **51,** 3–22.

——, 1997: Reply. *J. Atmos. Sci.,* **54,** 579.

——, E. Santoso, L. Berg, and J. Hacker, 1997: Boundary layer experiment 1996 (BLX96). *Bull. Amer. Meteor. Soc.,* **78,** 1149–1158.

Swinbank, W. C., 1968: A comparison between predictions of dimensional analysis for the constant-flux layer and observations in unstable conditions. *Quart. J. Roy. Meteor. Soc.,* **94,** 460–467.

Zilitinkevich, S., 1994: A generalized scaling for convective shear flows. *Bound.-Layer Meteor.,* **70,** 51–78.

——, and D. V. Chalikov, 1968: On the determination of the universal wind and temperature profiles in the surface layer of the atmosphere. *Atmos. Oceanic Phys.,* **4,** 294–302.